JOURNAL OF GEOPHYSICAL RESEARCH, VOL. 114, C04002, doi:10.1029/2008JC004821, 2009

Wave-mud interactions over the muddy Atchafalaya subaqueous clinoform, Louisiana, United States: Wave-supported sediment transport

S. Jaramillo,[1] A. Sheremet,[1] M. A. Allison,[2] A. H. Reed,[3] and K. T. Holland[4]

Received 24 March 2008; revised 30 October 2008; accepted 18 December 2008; published 10 April 2009.

[1] Near-bottom fluid-mud layers were observed during two experiments conducted on the muddy Atchafalaya inner shelf (subaqueous clinoform), Louisiana, United States. On the face of the subaqueous delta (4–7 m water depth, first experiment) fluid-mud layers are produced by seafloor liquefaction and resuspension forced by swells associated with cold front passages, and supported by near-bed wave-induced turbulence. The layers are episodic (lifetime of 9–12 h), form prior to significant postfrontal settling of sediment in the overlying water column, and flow seaward (downslope) at about 5 cm/s. Farther westward on the delta front (finer grain size, with negligible sand or coarse silt content, second experiment), similar wave-supported fluid-mud layers are observed to last longer (>2 days), show weaker alongshore (westward) flow of about 1–3 cm/s. The results suggest a sequence of near-bed sediment transport processes, triggered by frontal swell activity (bed liquefaction, resuspension and advection, modulated by the bathymetric characteristics of the clinoform) that contribute to the formation of clinoform stratigraphy of muddy subaqueous deltas.

Citation: Jaramillo, S., A. Sheremet, M. A. Allison, A. H. Reed, and K. T. Holland (2009), Wave-mud interactions over the muddy Atchafalaya subaqueous clinoform, Louisiana, United States: Wave-supported sediment transport, *J. Geophys. Res.*, *114*, C04002, doi:10.1029/2008JC004821.

1. Introduction

[2] Evidence based on the character of deposits in the geological record suggests that progradation on subaqueous mud clinoforms associated with large rivers (Amazon [*Cacchoine et al.*, 1995], Ganges-Brahmaputra [*Michels et al.*, 1998], Fly [*Walsh et al.*, 2004], and others) is dominated by fluid-mud layers which redistribute sediment from topset areas to foreset-bottomset regions. A subaqueous clinoform similar in morphology to these larger deltas [*Neill and Allison*, 2005] is developing on the inner Atchafalaya shelf, in the Northern Gulf of Mexico [*Roberts et al.*, 1980; *Wells and Kemp*, 1981; *Allison et al.*, 2000; *Walker and Hammack*, 2000; *Sheremet and Stone*, 2003; *Draut et al.*, 2005; *Kineke et al.*, 2006].

[3] The Atchafalaya River discharges into Atchafalaya Bay and adjacent shelf nearly 30% of the total water and sediment carried by the Mississippi River [*Mossa*, 1996], with an average suspended sediment load (calculated at Simmesport, LA, over the 1951–2000 period) of 84 million tons/a that includes 17% sand [*Allison et al.*, 2000]. The sediments are forming coarse-grained subaerial bayhead deltas at the mouth of the Atchafalaya and Wax Lake outlets into the Atchafalaya Bay [*Shlemon*, 1975; *Roberts et al.*, 1980; *Van Heerden and Roberts*, 1988] and a subaqueous muddy clinoform on the adjacent inner shelf [*Neill and Allison*, 2005] which is accreting vertically at rates up to 3.8 cm/a near the topset-foreset transition (rollover point). In addition, mudflats along the chenier coast west of the Atchafalaya Bay river mouth are experiencing progradation at rates ranging from 29 m/a [*Draut et al.*, 2005] to 60–80 m/a [*Roberts et al.*, 1989], in contrast to the rapid land loss trends observed along most of the Louisiana deltaic coastline.

[4] Recent studies [*Allison et al.*, 2000; *Kineke et al.*, 2006] conducted on the chenier coast west of Atchafalaya Bay during the peak Atchafalaya river discharge period of December–April (Figure 2 in the work of *Allison et al.* [2000]), suggest that sediment delivered via near-bottom fluid-mud layers is an important component of sediment transport on this subaqueous delta and is mainly driven by episodic high wave-current activity pulses associated with cold front passages over the same winter months. The scenario comprises two phases: (1) high waves associated with prefrontal onshore winds resuspend bottom sediments and break down the stratification of the water column derived from the river plume; and (2) poststorm stratification is restored and high-concentration, hindered-settling suspensions (e.g., fluid muds of suspended-sediment concentration greater than 10 g/l) are transported onshore by coastal

[1]Civil and Coastal Engineering, University of Florida, Gainesville, Florida, USA.
[2]Institute for Geophysics, University of Texas at Austin, Austin, Texas, USA.
[3]Seafloor Sciences Branch, Naval Research Laboratory, Stennis Space Center, Mississippi, USA.
[4]Mapping, Charting, and Geodesy Branch, Naval Research Laboratory, Stennis Space Center, Mississippi, USA.

0148-0227/09/2008JC004821$09.00

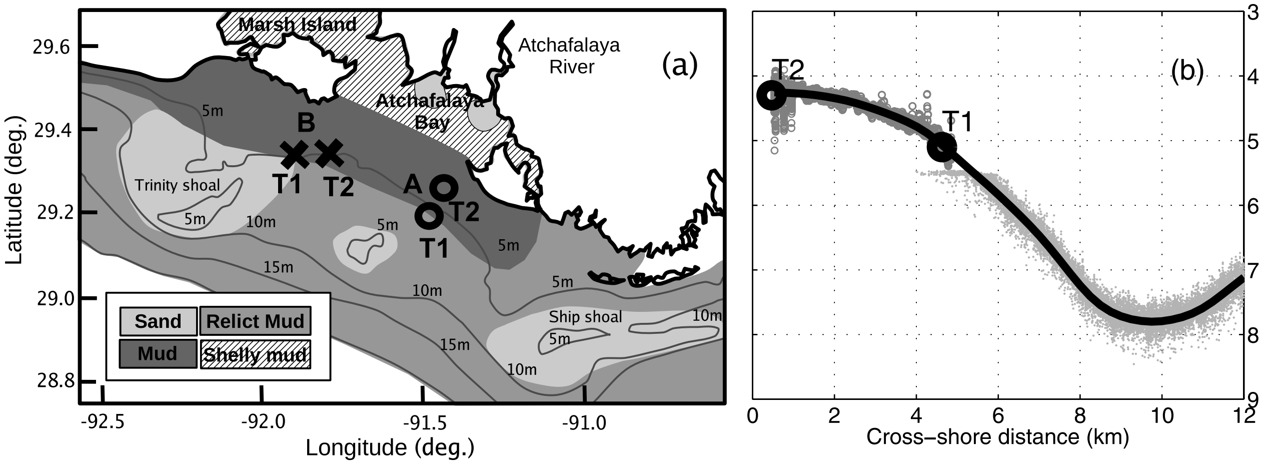

Figure 1. (a) Qualitative facies map of surficial sediments on the Atchafalaya shelf (based on C. F. Neill and M. A. Allison, unpublished data, 2005). Relict muds represent older Holocene Mississippi deltaic lobe deposits that are mantled ephemerally and discontinuously by modern mud layer less than 30-cm thick. The modern mud deposit represents the extent of the subaqueous mud clinoform delta [*Neill and Allison*, 2005] that merges west of −92.5 longitude into a concave, prograding shoreface deposit [*Draut et al.*, 2005]. The instrumented platforms (T1, T2) were deployed in two distinct configurations on the outer topset and foreset area of the clinoform. In Experiment A (1–14 March 2006, circles), the distance between the two platforms was about 4 km. In Experiment B (15–31 March 2006, crosses), the distance between the stations was about 5 km. (b) Smoothed estimate of bathymetry profile (continuous line) along a transect through and offshore of the two Experiment A sites (Figure 1a, circles). The light gray dots are fathometer readings from the R/V Pelican collected in March 2008 along the profile between T1 and T2. Because of the ships draft (4.5 m), fathometer readings were not obtainable for water depths less than about 5.5 m. To define the shallower section of the seafloor, fathometer data collected by NRL in May 2007 (dark gray circles) approximately 1 km west of the platform line are also shown. Survey data were checked against mean water level records at T1 and T2. The maximum slope is 0.0008, reached at x = 5 km, slightly offshore of platform T1.

upwelling and westward coastal currents ("Atchafalaya mud stream" [*Wells and Kemp*, 1981]). Wave-induced turbulence plays a key part in maintaining a near-bottom mud layer [*Kemp*, 1986]. The postfrontal onshore transport results in the observed mudflat accretion [*Kineke et al.*, 2006], but has not been linked to the high rates of sediment accumulation along the subaqueous delta front.

[5] The growth rate of the Atchafalaya subaqueous clinoform, 3 cm/a vertically (approximately 30 m/a horizontally) suggests that significant seaward sediment redistribution processes are also active. Limited observations to date have been made of originating mechanisms and sediment redistribution by mobile fluid-mud layers on deltaic clinoforms. Seaward flowing (downslope) fluid muds maintained by a balance of wave-boundary layer turbulence and stratification were shown to be a primary source to the nonclinoform midshelf mud deposit on the Eel River Shelf of California [*Traykovski et al.*, 2000]. Debris flows associated with gravity slumps and slides on the delta front triggered by pore pressurization caused by rapid sediment accumulation also have been observed, associated with the main Mississippi delta front [*Roberts et al.*, 1980; *Prior and Coleman*, 1984]. On the Amazon bottomset deposit, transport associated with fluid-mud layers has been attributed to fluid muds escaping bottom salinity front trapping on the topset area [*Cacchoine et al.*, 1995]. Both situations differ from the Atchafalaya by having steeper foreset slopes (1–5%), and water depths >40 m, where wave loading is a minor factor in generating fluid-mud layers. An exception to this is that bed liquefaction by hurricane wave loading has been observed to generate these failures on the Mississippi delta, on slopes of 1% or less [*Bea et al.*, 1983].

[6] On the microtidal (30-cm mean amplitude, 10-cm/s currents shallower than 10 m [*Wells and Roberts*, 1980; *Kemp*, 1986; *Walker and Hammack*, 2000]) Atchafalaya shelf, waves are the dominant forcing mechanism for sediment resuspension. Aside from tropical cyclones, the area has on average a low energy wave climate, with the notable exception of the period between February and April, when strong winds associated with atmospheric cold fronts pass over the area at 3 to 10-day intervals [*Mossa*, 1996; *Roberts et al.*, 1989; *Walker and Hammack*, 2000; *Kineke et al.*, 2006]. Prefrontal winds restrict the offshore extent of the Atchafalaya river plume, and in water of depth less than 10 m waves break down the stratification induced by the buoyant plume [*Allison et al.*, 2000; *Kineke et al.*, 2006]. Shallower than 5 m and during the postfrontal stages, suspended-sediment concentration in the water column can exceed 1 g/l with brief (<12 h) intervals of near-bottom fluid-mud suspensions (thickness <30 cm) with concentrations exceeding 10 g/l [*Allison et al.*, 2000].

[7] A series of field experiments were conducted on the muddy Atchafalaya Shelf (Louisiana, United States, Figure 1) in March 2006, to study wave-forced sediment transport, and associated mud-induced wave dissipation processes on the subaqueous clinoform. High-resolution

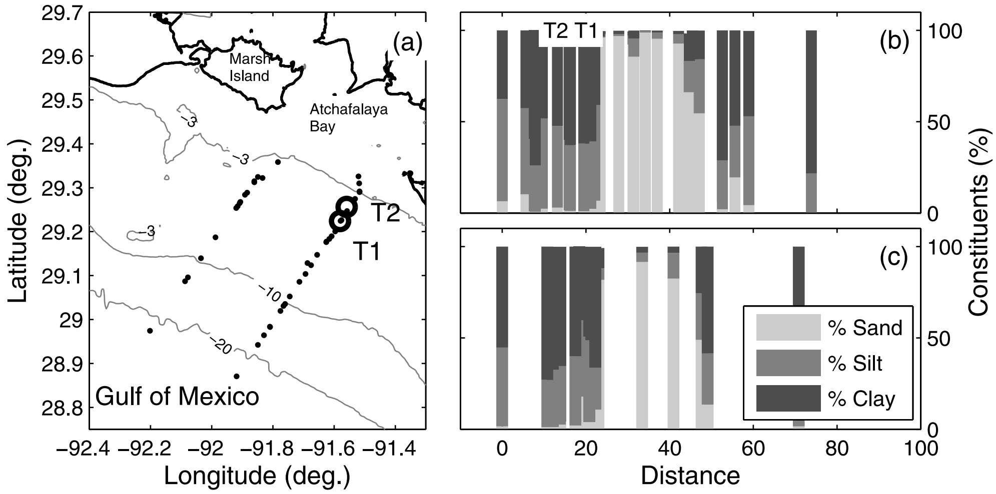

Figure 2. Sediment type distribution on the Atchafalaya Shelf. (a) Map of the shelf with sites where bottom sampling was done marked by dots (circles mark the location of T1 and T2 platforms, see also Figure 1). The distribution of sand, silt, and mud constituents versus distance from the shoremost sampling site, measured along (b) east transect and (c) west transect.

observations of wave, current, and sediment in the bottom boundary layer were collected, offering insight into near-bed and surficial sediment response to wave and current activity and its implication for observed clinoform strata formation patterns. In this paper, we present the experimental settings, sedimentological characteristics of the area, nature of frontal transport events that generate fluid-mud sediment transport, and the response of the surficial strata record to these events. The discussion provides the detailed context to examine wave dissipation processes (A. S. Sheremet et al., manuscript in preparation, 2009), as well as the effects of fluid-mud transport induced by frontal activity on the timing and sites of Atchafalaya sediment burial on the muddy clinoform.

2. Experimental Setting

2.1. Study Sites

[8] Two instrumented platforms (T1 and T2) were deployed between 15 January and 31 March on the inner Atchafalaya shelf of Louisiana (Figure 1). The instruments were serviced at about 14-day intervals, when they were brought on board ship for downloading data, replacing batteries, and cleaning biofouling from sensors. To avoid damage by shrimp trawler activity, the platforms were tethered to oil/gas platforms (10–25 m distance), and thus their placement was constrained by oil/gas platform availability.

[9] Although the duration of the entire experiment was over two months, here we discuss only observations collected during two 1-week time segments: "Experiment A," from 7 to 14 March, and "Experiment B," 15–22 March. During Experiment A the platforms were arranged in a cross-shore configuration (Figure 1, circles), with the inshore platform (4-m isobath) sited on the outer topset area of the subaqueous mud deltaic clinoform, and the offshore platform on the steeper foreset zone at about the 5 m isobath. These sites were picked based on CHIRP subbottom seismic data (Figures 1 and 10, line C, in the work of *Neill and Allison* [2005]), located 6.8 km to the west of the sites). Experiment B had a shore-oblique configuration, with both platforms located near the 5-m isobath, seaward of Marsh Island (Figure 1, crosses). These sites are midway between *Neill and Allison*'s [2005] CHIRP Lines A and B at foreset depths.

[10] Surficial sediments on the inner shelf seaward of Atchafalaya Bay are complex, with large adjacent patches of different sediment characteristics, and a large-scale alongshelf fining of Atchafalaya River-derived sediments: grain size grades from sandy and clayey silts in the east to silty clays with less than 5% sand and coarse silt in the west and along the chenier coast [*Neill and Allison*, 2005; *Draut et al.*, 2005]. This is also reflected in silt:clay contents in the mud fraction; greater than 3 to the east and decreasing westward opposite Marsh Island to about 0.2 to 0.5. This trend seems to be related to progressive sorting, as coarse materials (sand and coarse silt) accumulate closer to the riverine source when subjected to resuspension events, while finer sediments are transported further westward by coastal currents, with only brief interruptions during the cold front passages when postfrontal northerly winds advect sediments offshore [*Walker and Hammack*, 2000]. Based on USGS data at Simmesport, LA, the peak water discharge for 2006 was 8,770 m^3/s (on 30 March), slightly below the 1930–2007 average peak of 9,200 m^3/s.

[11] Based on data from previous studies showing inter-annual variations in sediment type at specific locations on the Atchafalaya inner shelf [*Allison et al.*, 2000], the distribution of sediment type on the shelf was sampled by the Naval Research Laboratory (NRL), Stennis Space Center on 3–5 May 2006 using a surface grab sampler. Figure 2 shows the results of sediment type analysis based on grab samples collected along two transects across Atchafalaya Shelf, the western one directly south of Marsh Island, crossing the shelf over the Experiment B site (see below), and the other passing over the sites of Experiment A (Figures 1 and 2). The samples agree with the qualitative

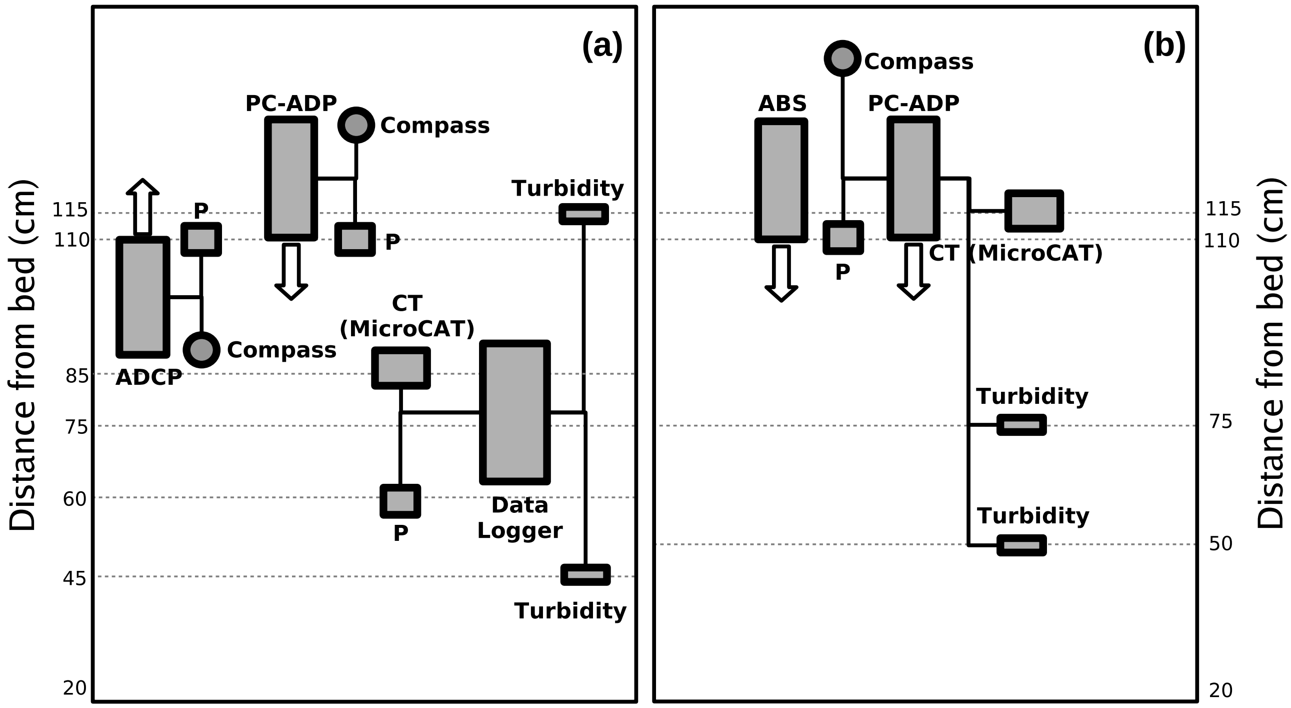

Figure 3. Schematic of configuration of platform (a) T1 and (b) T2, showing instruments deployed and their initial position with respect to the seabed. Arrows represent the direction of the acoustic beams.

picture in Figure 1. While the areas offshore of the 6-m isobath are dominantly sand (up to 95%), overall, during the period of our study, the surficial sediment in the experimental areas on the inner Atchafalaya Shelf appears to be a mixture of almost equal parts of silt and clay, with traces of sand (less than 5%) and shell gravel (less than 1%).The time span between the conclusion of the experiment (end of March 2006) and NRL sampling was a relatively calm period in the Northern Gulf of Mexico, with no major frontal storms. We do not expect the distribution of sediment grain size to have changed significantly, although it seems reasonable to assume that some consolidation would have occurred.

2.2. Instrumentation and Sediment Analysis

[12] Figure 3 shows a schematic of the instruments on the two platforms and their position with respect to the bed. The upper water column was monitored at platform T1 using an upward looking Acoustic Doppler Current Profiler (ADCP, 1-MHz Nortek AWAC), with transducers at approximately 110 cmab (Figure 3a). The ADCP recorded 2-min averages of velocity sampled at 2 Hz in 5–6 measurement bins (bin height 50 cm, blanking distance 45 cm), depending on the tidal phase. It also provided estimates of directional wave spectra based on 17-min measurement bursts, sampled free surface elevation at 4 Hz (surface track device) and pressure at 2 Hz, and logged data from its internal tilt sensor and compass.

[13] Platform T1 (Figure 3a) also housed a downward looking Sontek 1.5 MHz Pulse Coherent Acoustic Doppler Profiler (PC-ADP), that sampled the velocity profile and pressure at 2 Hz continuously for the entire duration of the experiment, in 17 3-cm bins covering the first 51 cmab (centimeters above the bottom), with a blanking distance of about 0.6 m from the instrument head, for a total distance from head to bottom of about 110 cm. This instrument also logged pressure recordings at 2 Hz and data from its internal tilt sensor and compass. Data from an additional Paroscientific pressure transducer (mounted at 60 cmab) sampling at 2 Hz in bursts of 2 h and 50 min every 3 h, were logged together with conductivity-temperature (Seabird MicroCAT, at 85 cmab), and information from two turbidity probes (Analite 195, McVan Instruments), mounted at approximately 45 and 115 cmab. A 1-min turbidity average was recorded at the end of a 3-h measurement burst.

[14] Platform T2 (Figure 3b) had an identical PC-ADP that in addition logged data from two OBSs (Downing and Associates model 3b Optical Backscatterance Sensor) located at 50 and 75 cmab, and a Seabird MicroCAT (conductivity and temperature) located at 115 cmab. The sampling scheme used at T2 was slightly different: 10-min long, 2-Hz measurement bursts every 30 min, sampling in 60 bins each 2-cm high, (10 cm blanking distance). Features associated with near-bottom suspended sediment (e.g., lutoclines) were also monitored on T2 with a single-frequency (700 MHz) Acoustic Backscatter Sensor (ABS, Marine Electronics, Isle of Guernsey). This instrument was located approximately at 100 cmab and measured the intensity of acoustic return from 0.9-cm bins covering a distance of 30 to 120 cm below the downward looking instrument head. ABS sampling was once every minute for the entire experiment duration.

[15] In energetic environments such as the Atchafalaya, the spatial resolution of the PC-ADP measurements can be constrained by “velocity ambiguity” effects. The PC-ADP calculates along-beam velocity based on the phase shift between two consecutive reflected acoustic pulses. Because the phase shift is determined up to multiples of 2π, velocity

measurements are unambiguous only if the true velocity is in the interval $[-\frac{1}{2} V_a, \frac{1}{2} V_a]$, where V_a is the ambiguity velocity, a value determined by the details of the instrument configuration and the speed of sound (V_a = 1.09 m/s in our measurements). If the magnitude of the true velocity is larger than $\frac{1}{2}V_a$, the measured values are wrapped (aliased) onto the interval $[-\frac{1}{2}V_a, \frac{1}{2}V_a]$. Sontek distributes an algorithm for resolving the ambiguity as a standard component of the PC-ADP software package. *Lacy and Sherwood* [2004] discussed this effect in detail and proposed an alternative approach that showed improved performance over the Sontek algorithm. Here, we resolve the velocity ambiguity using the algorithm developed by *Lacy and Sherwood* [2004].

[16] Turbidity sensors (OBS, Analyte) were calibrated for suspended sediment concentration in a laboratory tank using surficial bottom sediment and water samples (filtered) collected from the site. Standard concentrations were mixed using wet sediment samples and ranged from 10 mg/l to 300 g/l fluid muds; exact concentrations of these mixtures were determined later from filtered, dried and weighed sample aliquots. Turbidity sensors were immersed in the tank that was homogenized with slow-speed mixers and results were curve-fitted using the methods of *Kineke and Sternberg* [1992]. The principal (near-linear response) range of the instrument extended to about 30 g/l, with errors ranging from less than 1 g/l at concentrations lower than 10 g/l, to 2–5 g/l for concentrations above 30 g/l.

[17] At the beginning and end of each 14-day deployment, cores were collected from the platform sites using a 20 × 30 cm cross-section frameless box corer. Two subcores were collected from the resulting 20–40 cm long cores: a Plexiglas tray core (4.5 × 12 cm cross section) and a 10 cm diameter PVC round core. The former was X-rayed on board ship with a portable X-ray machine to allow examination sedimentary structures in near-surface sediments. The latter was extruded on board ship at 1 cm intervals and frozen for return to the laboratory. Water samples (50 l) and large volume (1–2 kg) surficial sediments were collected at the platform sites and stored frozen, in order to perform aforementioned laboratory calibration experiments. Extruded core sediment sample intervals were freeze–dried, ground, packed and sealed into 50 mm diameter Petri dishes in the laboratory. Porosities were calculated from water content (wet minus freeze dried weight) and assuming a particle bulk density of 2.65 g/cm^3. Down-core activities of short-period, particle-reactive radiotracers (^{210}Pb, ^{137}Cs, ^{7}Be) were determined by gamma spectrometry using Canberra low-energy Germanium planar detectors in order to examine age and source of surficial sediments. Samples were counted for 24 to 48 h immediately (to measure ^{7}Be with a 53 d half-life) and again at least 21 days after packing to allow ^{210}Pb activities to ingrow to secular equilibrium. Total ^{210}Pb activity was determined from the 46 keV photopeak and supported ^{210}Pb activities were determined by using averaged activities of the ^{226}Ra daughters ^{214}Pb (295 and 352 keV) and ^{214}Bi (609 keV). ^{137}Cs and ^{7}Be activities were also determined for these cores using the 661.6 (Cs) and 477 keV (Be) photopeaks. Detector efficiencies for this geometry were calculated using a natural sediment standard (IAEA-300 Baltic Sea sediment); detector backgrounds at each energy of interest were determined using Petri blanks and high-level sources [*Cutshall et al.*, 1983].

[18] In addition to the grain size samples collected by surficial grab on 3–5 May 2006, bearing strength of the upper 80–100 cm of the seafloor was measured for 12 of these stations. Bearing strength was determined from three successive free-fall deployments of a lance-type penetrometer (STING MKII) developed by Ago Environmental Ltd. Victoria, BC. The penetrometer is attached to a rope, deployed by hand, lowered over the side of the boat and into the water and then allowed to free fall to the bottom. The configuration of the penetrometer was a 2 m long shaft with a 70 mm diameter foot. Acceleration and pressure changes are recorded at 2 KHz during the deployment time interval. The acceleration data are then converted to bearing strength by accounting for the drag forces acting on the penetrometer and computing the force exerted by the sediment upon the penetrometer.

3. Results

[19] Tidal circulation at the experimental sites on Atchafalaya Shelf is characterized by mean 30-cm surface elevation amplitudes and nearly vertically uniform currents that rarely exceed 30 cm/s. The main tidal constituents, O1 (period 25.82 hr), K1 (period 23.93 hr), and M2(12.4 hr), have a progressive-wave component propagating alongshore (approximately eastward) and a nearly standing-wave component (cross-shelf, northward [e.g., *DiMarco and Reid*, 1998]). During the experiments, cold fronts passing through the area generate episodic currents rarely exceeding 30 cm/s and typically within the first 2-m below water surface, associated with surface elevation variations of less than 20 cm.

[20] This paper discusses two time intervals during experiments A and B, when significant correlations were observed between bottom sediment processes (e.g., fluid-mud layer dynamics) and wave-current activity. Experiment A captured a particularly energetic perturbation associated with a cold front that passed over the Atchafalaya shelf between 7 and 14 March 2006. In contrast, Experiment B was characterized by low energy atmospheric and sea conditions, with only occasional weak pulses of wave activity.

3.1. Experiment A

[21] The main atmospheric event during the second week of Experiment A (7–14 March) was a cold front that was stationary over the area between 7 and 10 March, when it started moving slowly eastward. The front produced fairly intense (10–15 m/s) southerly winds (Figures 5a and 5e), with a short period of reduction to about 5 m/s on 10 March, corresponding to the front passing over the observation site. To correlate wave activity with bottom sediment processes, following *Sheremet and Stone* [2003], we distinguish here between "seas" (waves with frequency >0.2 Hz) and swells (frequency <0.2 Hz, peak frequency 0.10–0.13 Hz). The two frequency bands have different dynamics: short-fetch seas are generated by local wind forcing, whereas swells require a long fetch to develop and thus are less responsive to local winds. More importantly for this work, in 5-m depth of water a typical swell wave (8-s period, wavelength

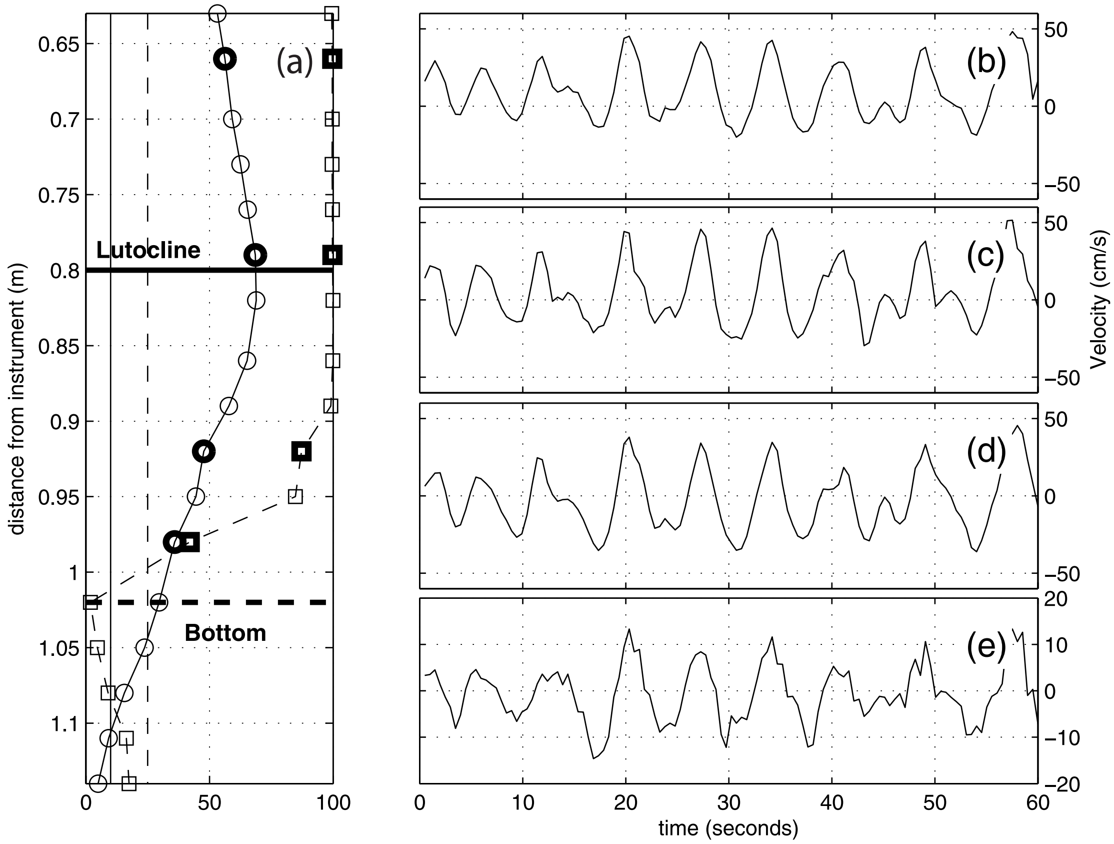

Figure 4. Sample of velocity time series and vertical profile of data quality indicators for the PC-ADP at T1, on 11 March 03:00 h UTC, Event "2," Experiment A. (a) Vertical structure of ping-to-ping correlation (PPC, squares) and signal-to-noise ratio (SNR, circles, averaged over 1 min). The fluid-mud layer extends between approximately 80 cm to 100 cm from the instrument head. The signal is consistently above the minimal acceptable levels suggested by the manufacturer (Sontek), marked by dashed (PPC) and continuous (SNR) vertical lines. (b–e) Sample time series of S-N velocity at four levels (marked by thick-line symbols on Figure 4a): topmost measurement bin, top and middle of the fluid-mud layer, hydrodynamic bed (bin position 66, 79, 92, and 98 cm from instrument head). Vertical scale on Figure 4e is not the same as in Figures 4b–4d.

approximately 50 m) is in shallow water and interacts strongly with the seafloor.

[22] The response of the bed sediment to the 7–14 March storm shows a strong correlation with swell variations. Sustained frontal winds were accompanied by energetic seas (1-m height at the peak of the storm), with energy variations following closely wind speed variability; swell height peaked at about 1.5-m just after the arrival of the front (label "1" in Figures 5a and 5e), decayed as the front passed over the experimental site, and increased again briefly after the front (label "2").

[23] Bed-sediment motion can in principle be inferred based on PC-ADP and ABS velocity and acoustic backscatter measurements. Surfaces of large sound-velocity gradient of (e.g., lutocline, bottom) have a strong acoustic backscatter; if the near-bed velocity is large enough to allow for reliable measurements, the level where the mean velocity becomes zero (hydrodynamic bottom) should also closely correlate with bottom position. However, a high suspended-sediment content may dissipate the acoustic signal within the sediment layer to the point where velocity measurements are no longer reliable. Figure 4 shows sample time series of velocity collected by the PC-ADP at T1, on 11 March 03:00 h UTC, during an event that exhibited high-concentration suspension. Standard data quality measures, ping-to-ping correlation and signal-to-noise ratio (Figure 4a), are within the recommended values throughout the measurement range. Based on this result, we identify here maximum-backscatter elevation with the seafloor position when coincident with the hydrodynamic bottom, and as the lutocline, when reliable nonzero velocity values are recorded below its level.

[24] At platform T1 (sited on the foreset area of the clinoform, Figure 1b), the elevation of the acoustic and hydrodynamic bottoms agree during prefrontal and post-frontal stages (7–9 March and from 12 March on, respectively). However, there are two occurrences of about 1 day each (9–10 March; and 11 March, events labeled "1" and "2" on Figure 5) associated with the two peaks of wave activity, when the acoustic bottom is 10–15 cm higher than the hydrodynamic one, with mean current velocities up to 5 cm/s recorded below the lutocline (acoustic bottom). During these events, the turbidity sensors at T2 (located at 50 and 75 cmab) recorded peak concentrations between

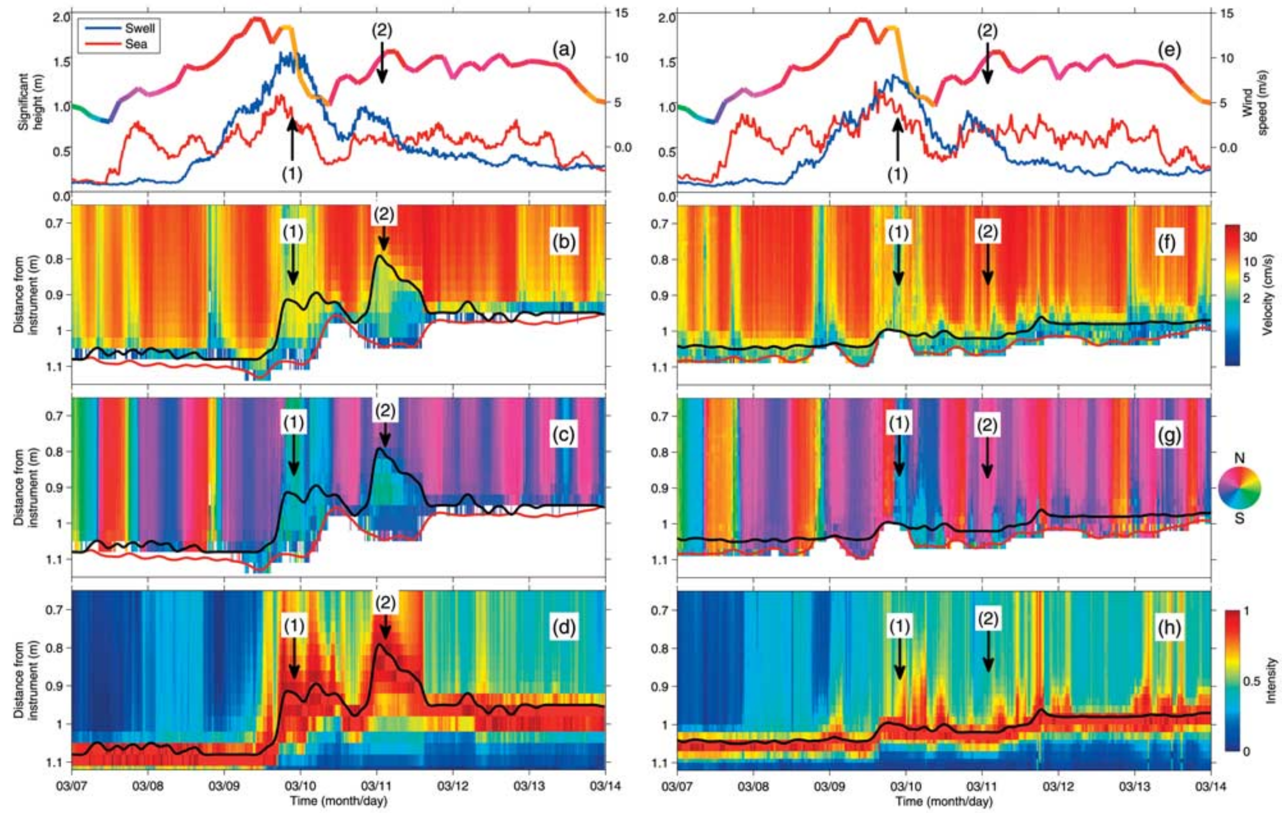

Figure 5. Observations of wave and near-bottom currents and sonar signal intensity (PC-ADP), during the 10 March storm in Experiment A. (left) Platform T1. (right) Platform T2. (a, e) Swell (frequency <0.2Hz) and sea (frequency >0.2 Hz) calculated from the PC-ADP pressure sensor; (b, f) vertical structure of near-bottom current velocity (logarithmic scale); (c, g) near-bottom current direction; (d, h) echo intensity (normalized between 0 and 1). Backscatter intensity is not corrected to account for signal attenuation due to suspended sediment concentration. Black line, approximate position of maximum reflection surface; red line, approximate position of zero velocity (hydrodynamic bottom). Labeled arrows mark events discussed in the text.

1–3 g/l. Although measured too high above the bed to provide a direct confirmation, these values support the assumption that the mobile and relatively dense bottom layers are fluid muds (e.g., concentration in excess of 10 g/l), and we will refer to them as such in the following discussion. The interpretation of the acoustic bottom as a lutocline is also supported by the lower-frequency and higher-resolution (0.9 cm bin height) ABS data collected during Experiment B, see section 3.2.

[25] The first fluid-mud event at T1 (label "1," Figure 5) developed rapidly, reaching its maximum thickness within approximately 1 h, correlated to a significant increase in swell height (from 1 to 1.5 m). Just before the expansion of the first fluid-mud event, the hydrodynamic bottom estimate (Figures 5b–5d, red line) separates from the acoustic bottom. In this case the evolution is opposite to what one would expect in the case of a developing lutocline when the position of the acoustic bottom rises. The position of the acoustic bottom remains unchanged, instead, the hydrodynamic bottom falls by about 3–6 cm below the acoustic bed (see Figure 6, label "Liquefaction"). A surficial bed layer of 3 to 6-cm thickness is mobilized and starts flowing downslope (southward) with a mean velocity of 3–5 cm/s (Figures 5b, 5c, and 6a). Remarkably, close to the deepest measurement cell RMS wave orbital velocity exceeds 10 cm/s (Figure 6b and Figure 7), suggesting that wave motion penetrated at least 6–10 cm below the acoustic bottom, located at approximately 105 cm from instrument head (Figure 7a). This sequence of events is consistent with swell-induced bed liquefaction/failure followed by the downslope sliding of the layer. The subsequent expansion of Event 1 might be due to either to local resuspension or to the arrival of upslope suspended sediment delivered via a near-bottom gravity flow.

[26] During Event "1" the instrument platform sank into the bed by about 10 cm (compare the bottom position on 9 March to that of 11 and 13 March, Figure 5d). The change in bed position relative to the instruments was verified by the difference between the average pressure during the first and second half of the experiment, and caused slight but measurable changes in PC-ADP magnetic compass heading.

[27] The second fluid-mud event at T1 occurred in the wake of frontal passage on 11 March (Figure 5, label "2"), under weaker swell (0.8-m significant height). The thickness and mean velocity of the second fluid-mud event peaked at about 25 cm and 5–10 cm/s, respectively. The

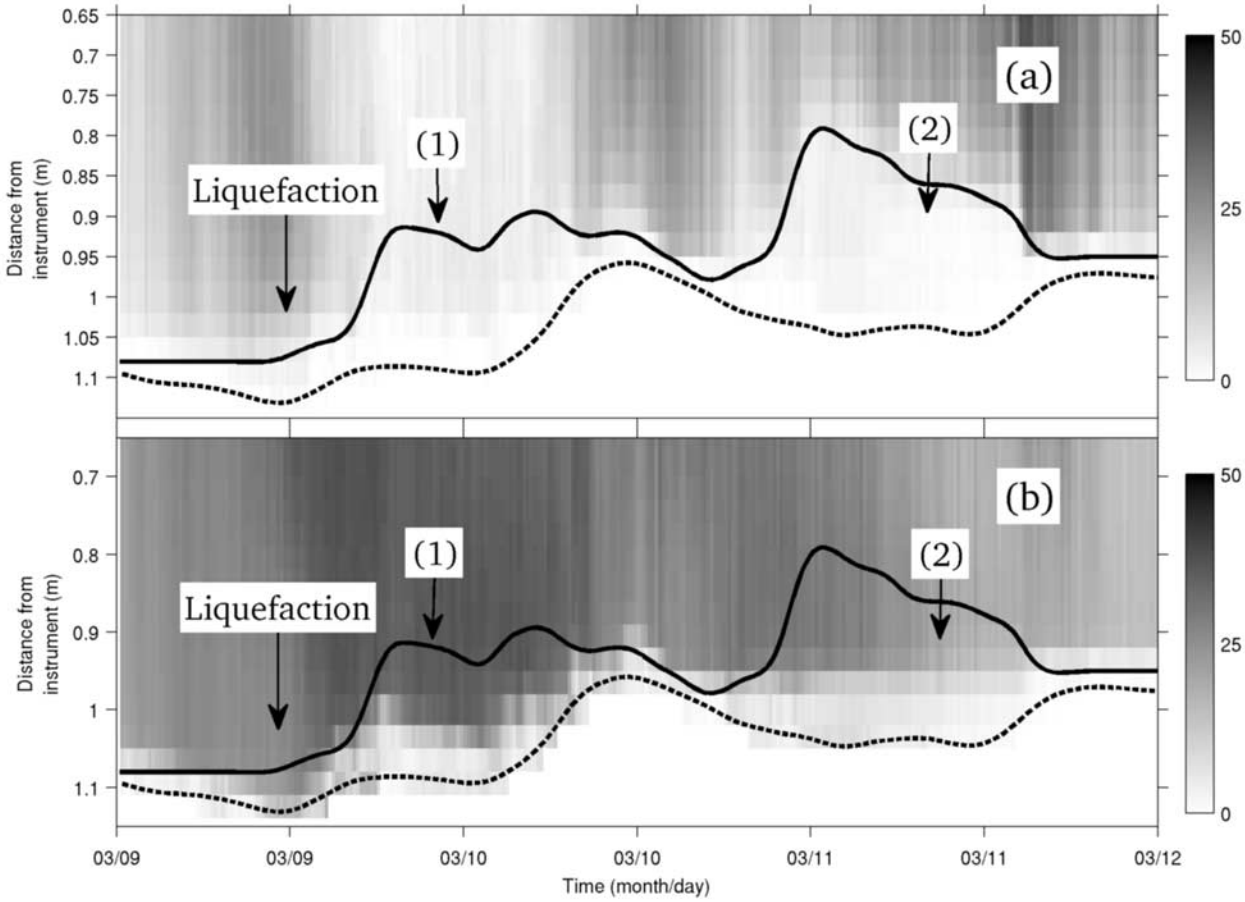

Figure 6. Observations of the vertical structure of (a) mean currents velocity and (b) RMS wave orbital velocity, measured by the PC-ADP at T1 during the 7–14 March storm, Experiment A. Solid line, acoustic bottom; dashed line, hydrodynamic bottom. Labeled arrows mark events discussed in the text.

flow was seaward (southward), opposite to the flow direction of the overlying water column. No sinking of the instrument platform was observed during this event. Wave activity (Figure 6b) was confined to the layer bounded by the lutocline and the hydrodynamic bottom, suggesting a lesser role for wave-induced bed liquefaction.

[28] Figures 5e–5h show PC-ADP records from the upper topset site of platform T2 (compare with T1, Figures 5a–5d). Differences in acoustic and hydrodynamic bottom position at T2 during Events "1" and "2" (Figure 5b) are sufficiently small (1–2 PC-ADP measurement cells), to be regarded as within instrument error (if fluid-mud layers were present at T1, they are less than 10 cm thick). The ABS record at T2 (not shown) does not indicate the presence of a lutocline. Platform T2 did record an abrupt 5-cm sinking at the beginning of the storm and magnetic compass fluctuations, likely associated with the liquefaction of the bed by wave activity. The differences in sinking depth are likely due both to different platform design (weight and surface area of the feet) and to different geotechnical bed properties.

[29] The relatively small flow velocity of the mud layers observed and the fact that the direction of the flow is consistently downslope (southward) suggests that Events "1" and "2" are wave-supported gravity flows [e.g., *Parsons et al.*, 2007]. Following *Wright et al.* [2001] and *Scully et al.* [2002], we assume that the gravity flow is sustained by the balance between the downslope negative buoyancy of suspended sediment and frictional drag force, i.e.,

$$B \sin\alpha = C_d U u_g, \quad \text{with} \quad B = gs\int_0^\delta c\,dz, \quad \text{and} \quad U = \sqrt{u_g^2 + u_w^2 + v_c^2}, \tag{1}$$

where the symbols employed are: α, the bottom slope; B, buoyancy of the mobile mud layer; C_d, the frictional drag coefficient at the bottom of the layer; g, the gravitational acceleration; s, submerged weight of sediment relative to sea water; δ, layer thickness; and c, the sediment volume concentration. The effects of waves and alongshore current are included in the maximum velocity: u_w and v_c are the RMS wave orbital velocity and the alongshore current at the top of the wave boundary layer. If the Richardson number is maintained at its critical value ($Ri_{cr} = 0.25$ [*Trowbridge and Kineke*, 1994; *Wright et al.*, 2001]), the gravity flow velocity can be estimated as

$$u_g = \beta U = \beta\sqrt{\frac{u_w^2 + v_c^2}{1-\beta^2}}, \quad \text{with} \quad \beta = \frac{Ri_{cr}\sin\alpha}{C_d}. \tag{2}$$

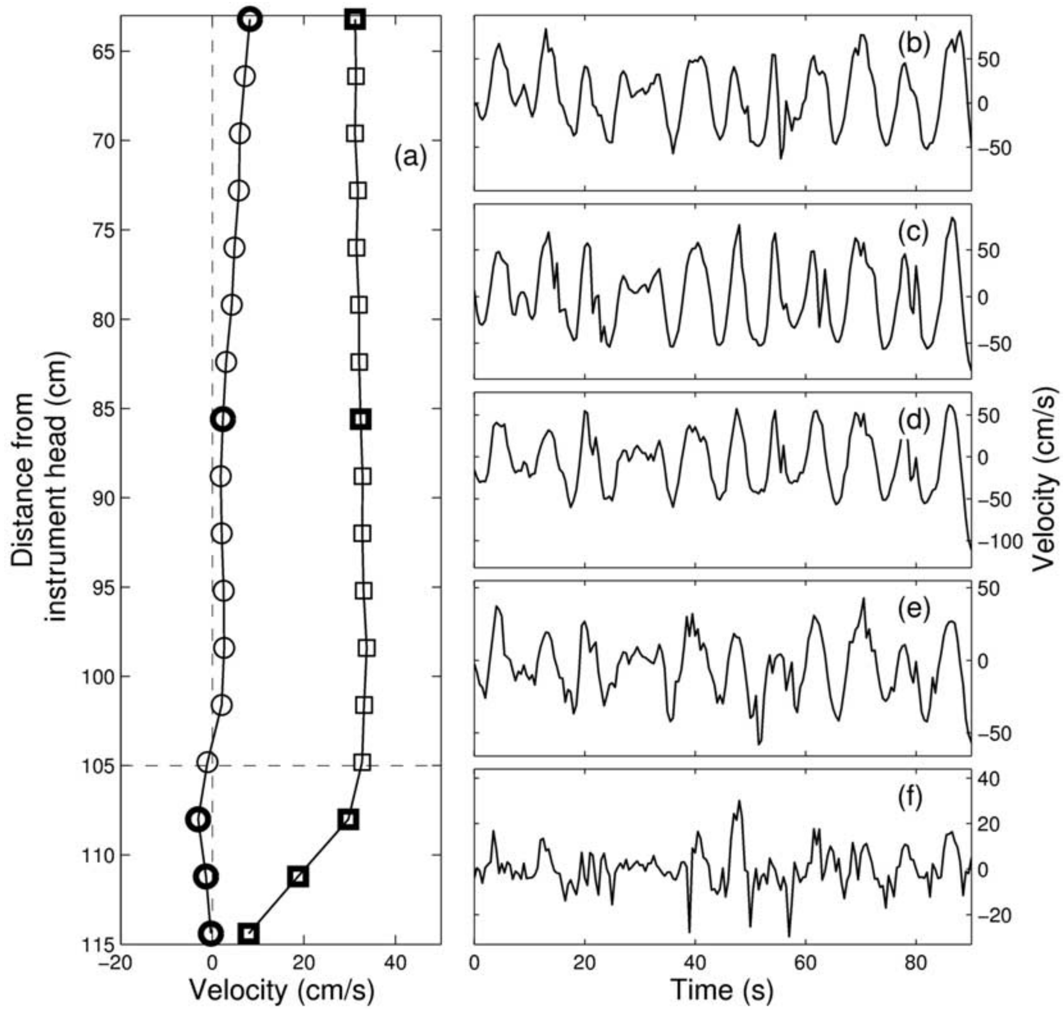

Figure 7. Velocity measurements (PC-ADP) at T1, on 9 March 12:25 h UTC, during Experiment A (label "Liquefaction" in Figure 6). (a) Vertical structure of RMS orbital velocity (10-min average, squares) and mean velocity (circles). The position of the acoustic bottom is below 105 cm from the instrument head (dashed horizontal line, solid line in Figure 6). (b–f) Sample time series of velocity at five levels (marked by thick-line symbols on Figure 7a): 66 (topmost cell), 86, 108, 111 and 114 cm from instrument head. To highlight the similarity between signals, the limits of the velocity axes on Figures 7b–7f are not the same.

[30] We apply this model to estimate the gravity flow velocity u_g for the two fluid-mud events observed in Experiment A. We limit the analysis to several segments of the entire duration of the event. For Event "1" (Figure 5), we discuss only the first half of its duration, 9 March 18:00 h to 10 March 02:30 h, marked by a rectangle in Figure 8e, to avoid complications due to the settling of the instrument platform. For Event "2," we discuss only the segment covering the initial expansion, when the layer reaches maximum thickness and flow velocity (early morning of 11 March, Figure 9). Estimating the bottom slope at α = 0.0006 and using a drag friction coefficient of C_d = 0.003 [*Wright et al.*, 2001; *Scully et al.*, 2002] with Ri_{cr} = 0.25 yields β = 0.05, which matches the order of magnitude of the observations (e.g., $u_w \simeq 30$ cm/s, and $u_g \simeq 2$ cm/s, Figure 9). This value suggests that events "1" and "2" never reach the status of a self-sustaining (autosuspension) turbidity flow, and are likely wave-supported flows. During the first half of Event "1" the lutocline and the top of the wave boundary layer (WBL, Figures 8a and 8e) coincide, both located near the measurement cell at 95 cm from the instrument head. The gravity flow velocity u_g derived using equation (2) is consistent with estimates of the mobile mud layer downslope velocity in both Event "1" and the expansion stage of Event "2" (Figures 8d and 9d); however, at its peak, the Event "2" layer is approximately twice as thick as the WBL (Figures 9a–9c). During the second half of this event, the same analysis (not shown) indicates that the lutocline returns to the level of the WBL top, with an observed flow velocity below the model critical velocity u_g, consistent with the depositional trend, and the decrease in wave forcing.

3.2. Experiment B

[31] During Experiment B (Figure 10) observations of PC-ADP and ABS backscatter intensity at T2 showed

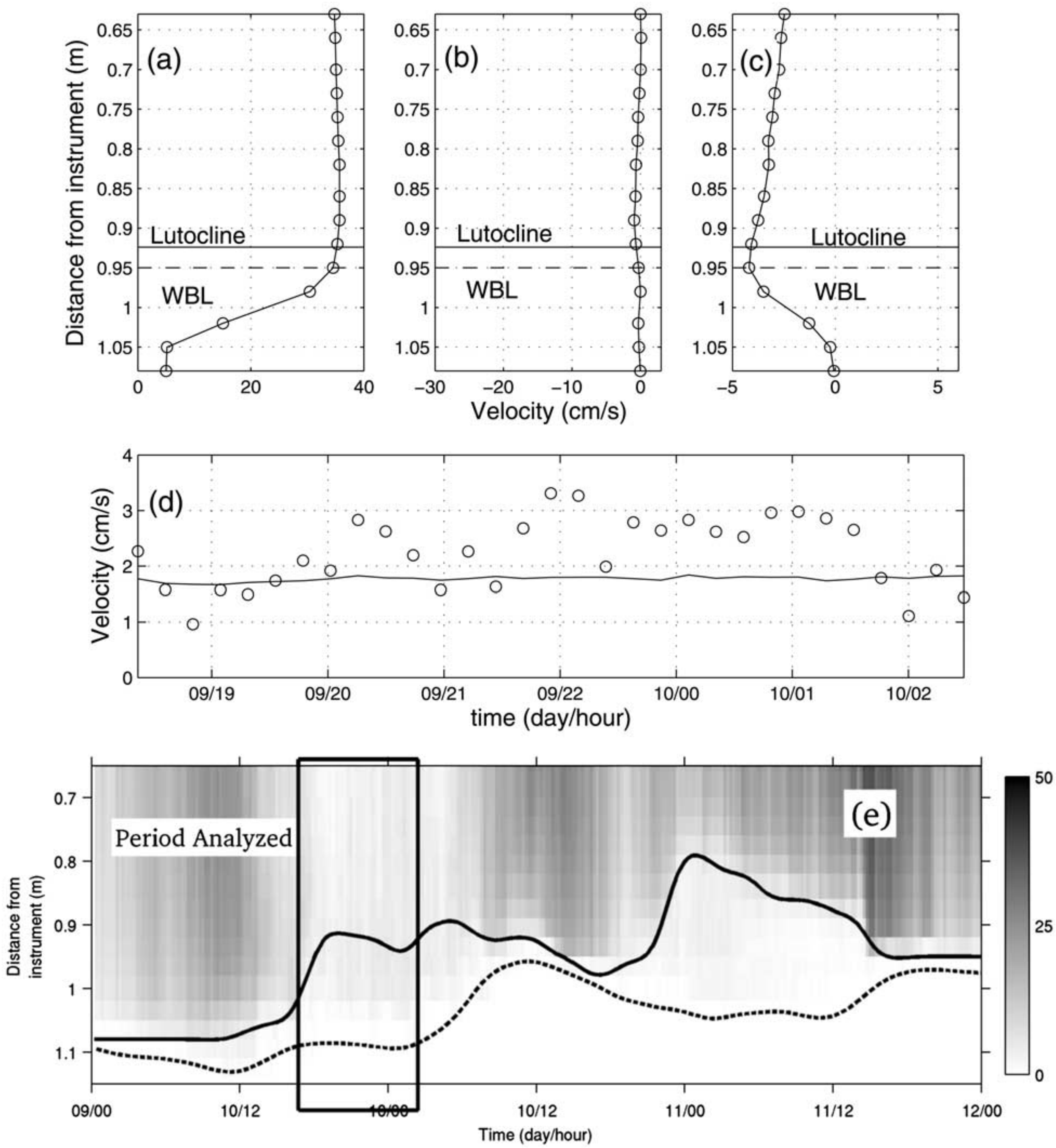

Figure 8. Observations of cross-shore (S-N) velocity (9 March 18:00 to 10 March 2:00 UTC) compared to downslope velocity of a critical gravity flow [*Wright et al.*, 2001, equation (2)]. (a) RMS wave orbital velocity u_w; (b) alongshore (E-W) current velocity v_c; (c) cross-shore (S-N) current velocity. Velocities shown in Figures 8a–8d represent 6-h averages (the duration of the entire period analyzed). The approximate position of the WBL (dashed line) and the lutocline (continuous line) are also marked on Figure 8. (d) Critical gravity flow velocity u_g (continuous line) and observed cross-shore (S-N) flow velocity (circles, 20-min averages, vertically averaged over the extent of the WBL). (e) Vertical structure of current velocity measured by the PC-ADP at T1 during Experiment A (e.g., Figure 5b), with the period analyzed in Figures 8a–8d marked by a rectangle.

persistent, 20 to 30-cm thick fluid-mud layers with a well-developed lutocline, moving slowly, with mean-current velocities well below 3 cm/s, (e.g., label "1" in Figure 10b) and in the direction of the overlying water column flow (Figure 10c). Occasional pulses of tidal bottom currents eroded the lutocline exposing the bottom (e.g., label "2" in Figure 10). Wave activity was mostly confined to short waves, sometimes exceeding 1-m significant height (Figure 10a). The single larger swell event on 20–21 March (Event "3," Figure 10a) caused an expansion of the fluid-

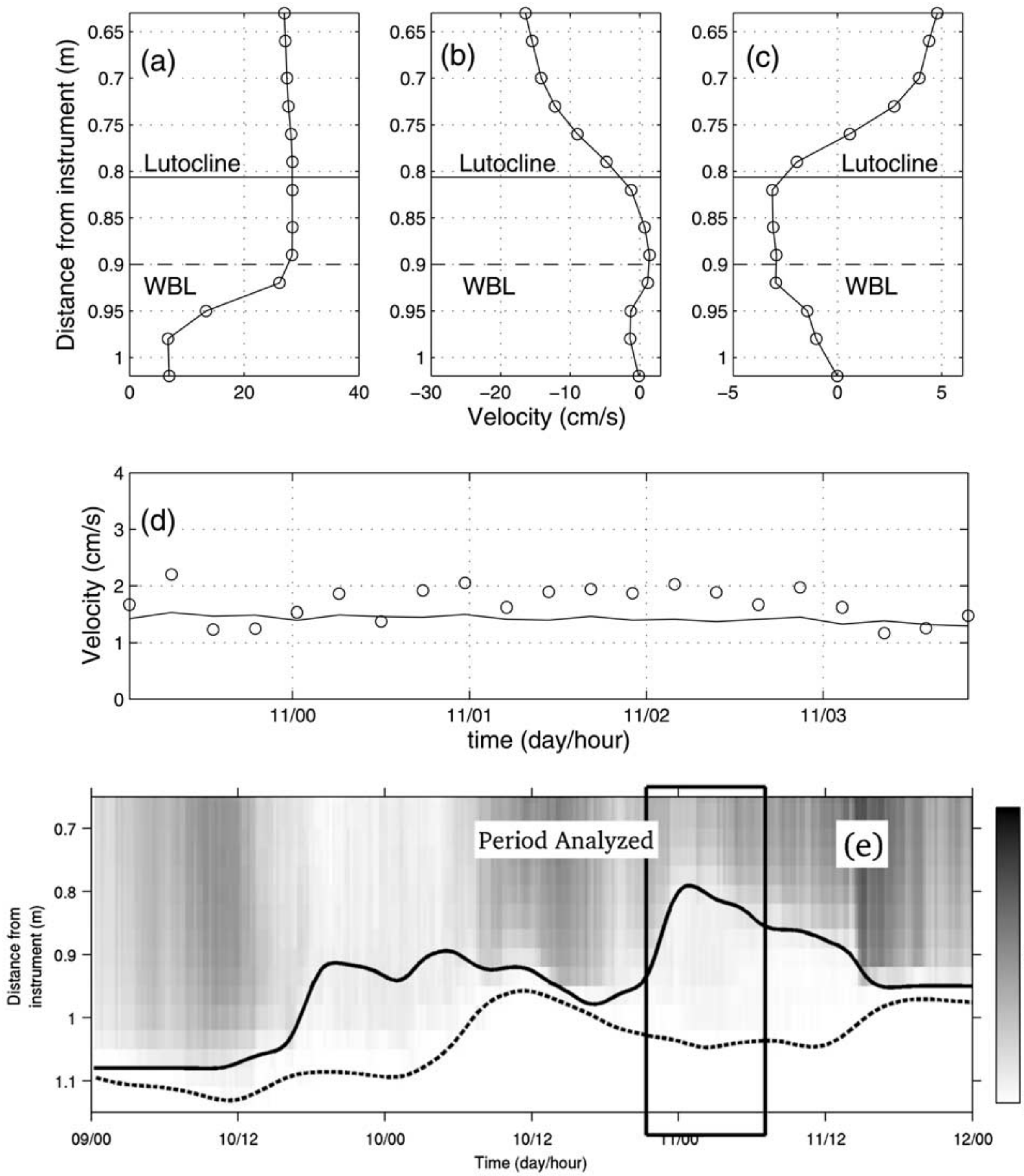

Figure 9. Observations of cross-shore (S-N) velocity (10 March 23:00 to 11 March 4:00 UTC) compared to downslope velocity of a critical gravity flow (see Figure 8). (a) RMS wave orbital velocity u_w; (b) alongshore (E-W) current velocity v_c; (c) cross-shore (S-N) current velocity. Approximate position of the WBL (dashed line) and the lutocline (continuous line) are also marked on Figure 9. (d) Critical gravity flow velocity u_g (continuous line) and observed cross-shore flow velocity (circles). (e) Vertical structure of current velocity measured by the PC-ADP at T1 during Experiment A (e.g., Figure 5b), with the period analyzed in Figures 9a–9d marked by a rectangle.

mud layer and a backscatter intensity reduction of the acoustic lutocline surface consistent with reduction in fluid-mud concentration.

[32] In this data set, due to low current velocities, inside the fluid-mud layer the velocity decays too fast to allow for identifying the zero-velocity level as the seabed (e.g., in Figures 10c and 10d); the ‘‘hydrodynamic bottom’’ is simply a curve roughly parallel to the lutocline. This situation highlights the usefulness of the ABS, which having lower frequency (700 kHz) and higher resolution

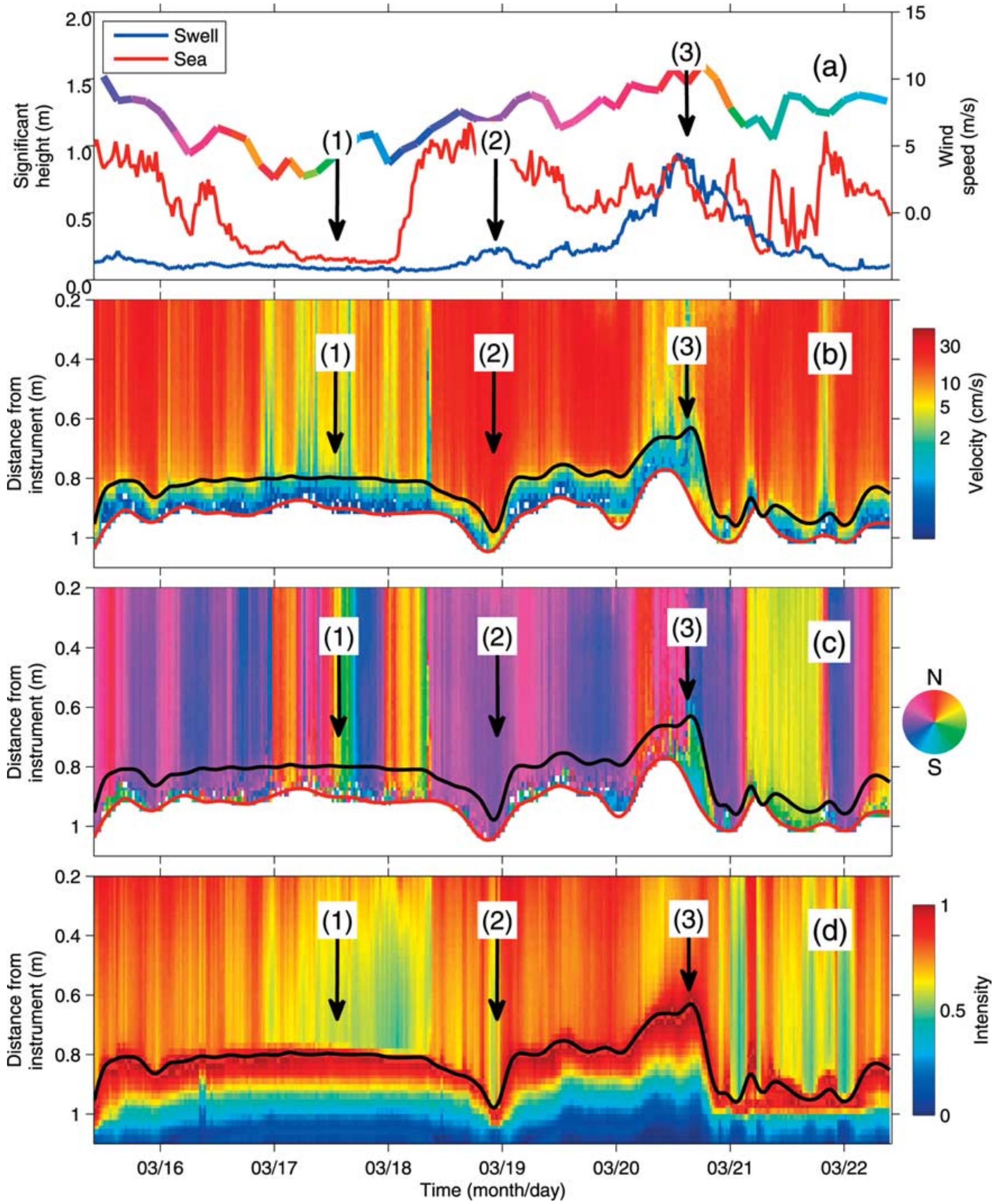

Figure 10. Observations of waves and near-bottom currents and sonar signal intensity (PC-ADP), during Experiment B at platform T2. (a) Significant height of swell (frequency <0.2Hz) and sea (frequency >0.2 Hz) estimated based on PC-ADP pressure data; (b) vertical distribution of current velocity; (c) current direction; (d) PC-ADP backscatter intensity (normalized between 0 and 1). Black line in Figures 10b–10d marks the approximate position of maximum reflection surface. Red line on Figures 10a–10c marks the location of hydrodynamic bottom (in this case, clearly not the true bottom). Labels mark periods characterized by different fluid-mud regimes: (1) settling; (2) fluid-mud layer is eroded; (3) peak of fluid-mud thickness, coinciding with swell peak; expansion due to resuspension by waves.

(0.9 cm depth bins) than the PC-ADP, provides a sharp image of the lutocline and bed position (Figure 11a). As was the case in Experiment A, RMS wave orbital velocity is significantly larger than the mean current velocity and as a result penetrates deeper into the mud layers (compare Figures 10b and 10c with Figure 11b). The two OBS deployed at T2 in this experiment were placed too high in the water column to observe the lutocline, which was about 20–25 cmab most of the time. However, during the mud-layer expansion of 20 March associated with the swell event

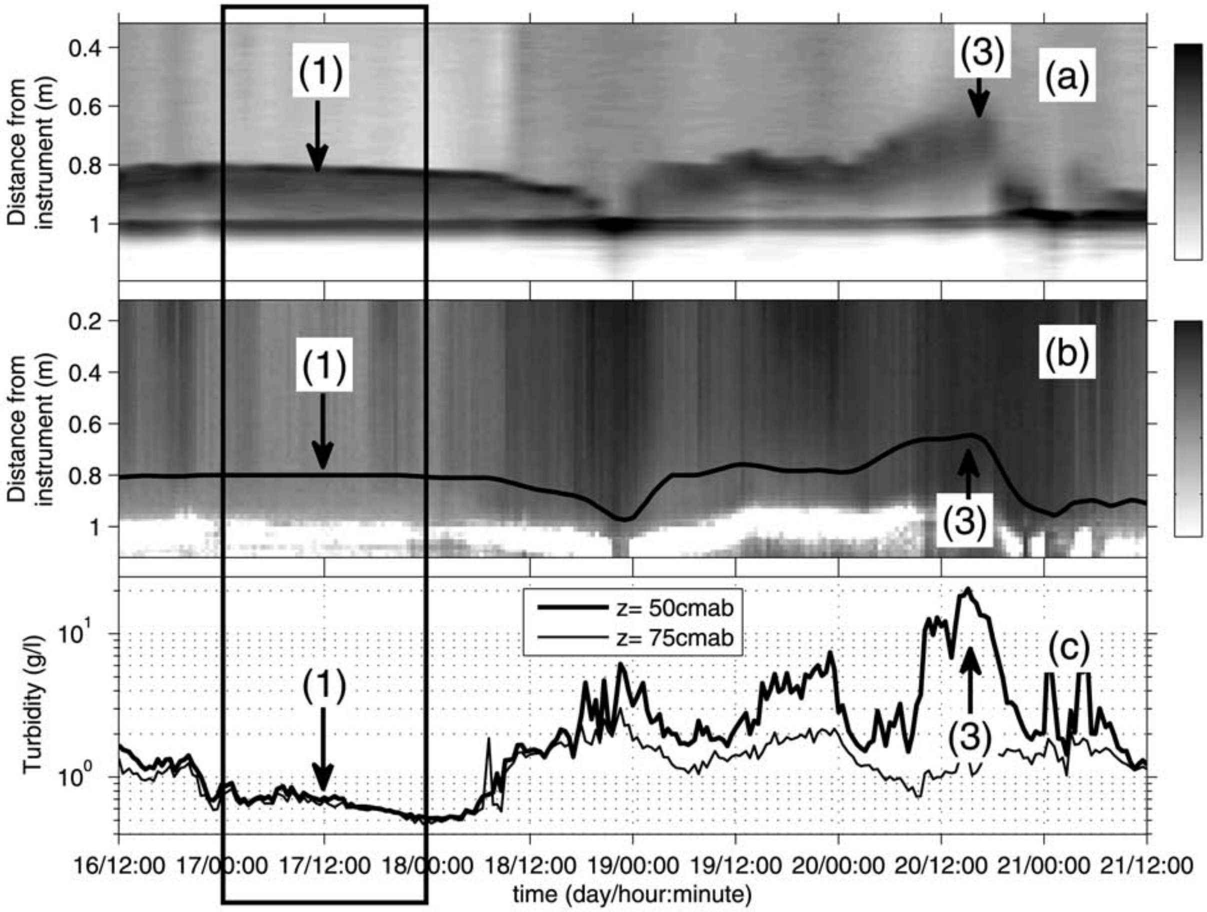

Figure 11. Suspended-sediment concentration recorded by the OBS at T2 during Experiment B, March 2006. (a) ABS backscatter intensity (see also Figure 10d). (b) RMS wave orbital velocity, the bold line marks the approximate position of maximum reflection surface. (c) Suspended-sediment concentration recorded by the two OBS. Labels "1" and "3" correspond to the events marked on Figure 10. To simplify Figure 11, Event "2" is not marked. The rectangle marks the event detailed in Figure 12, and discussed in the modeling section for Experiment B.

(label "2" in Figures 10 and 11), the lutocline rose to about 40 cmab, within 10 cm distance of the lowest OBS (assuming no tripod settling during the deployment), which registered suspended-sediment concentration values between 10 and 20 g/l (Figure 11c).

[33] Event "1" in Experiment B, Figure 10 (evening of 17 March to morning of 18 March), is remarkably persistent under apparently very low forcing (mean current less than 3 cm/s within the mud layer, Figures 10b and 10c), and flowing in the alongshore direction (roughly E-W). The layer maintained an almost constant lutocline height (only 3-cm decrease) over approximately 24 h (noon 17 March to noon 18 March, Figure 11). The weak forcing and the low slope suggests that the sediment was maintained in suspension by a balance of wave-induced turbulence and settling. *Vinzon and Mehta* [1998] found that under such a balance the height H of the lutocline can be expressed as

$$H = 0.65\left[\frac{\left(a_b^3 k_r\right)^{3/2}}{T^3\frac{\rho_s-\rho_w}{\rho_w} g w_s C_v}\right]^{1/4}, \qquad (3)$$

where a_b is the amplitude of the wave orbital velocity at the bottom; k_r is the hydraulic roughness; T is a characteristic (e.g., peak) wave period; ρ_s is the particle granular density, and ρ_w is the water density; w_s is the settling velocity; C_v is the mean volumetric concentration of solids in suspension, i.e., dry sediment volume per unit volume of sediment-water mixture. For numerical simulations, we used $\rho_s = 2650$ kg/m^3, ρ_w = 1015 kg/m^3; k_r = 3 cm [*Vinzon and Mehta*, 1998]. Given the low advection velocities, the nearly stationary lutocline height and suspended-sediment concentrations above the lutocline (Figure 12b), and the maximum values recorded by the lowest OBS, the concentration within the fluid-mud layer was estimated to be constant at about 50 g/l; with a diameter of the fundamental particle (whose density is ρ_s) $d_0 = 3\mu\ m$, a floc characteristic diameter $d = 60\mu\ m$, and fractal dimension n_f = 2.15 [e.g., *Kranenburg*, 1994]. The resulting values of the mud-floc density [*Hsu et al.*, 2007] and mean volumetric concentration are ρ_m = 1233 kg/m^3, and C_v = 0.04. Wave amplitude a_b was estimated as the vertical mean of the RMS orbital velocity (Figure 11b) at between the bottom and the height of the lutocline (inferred

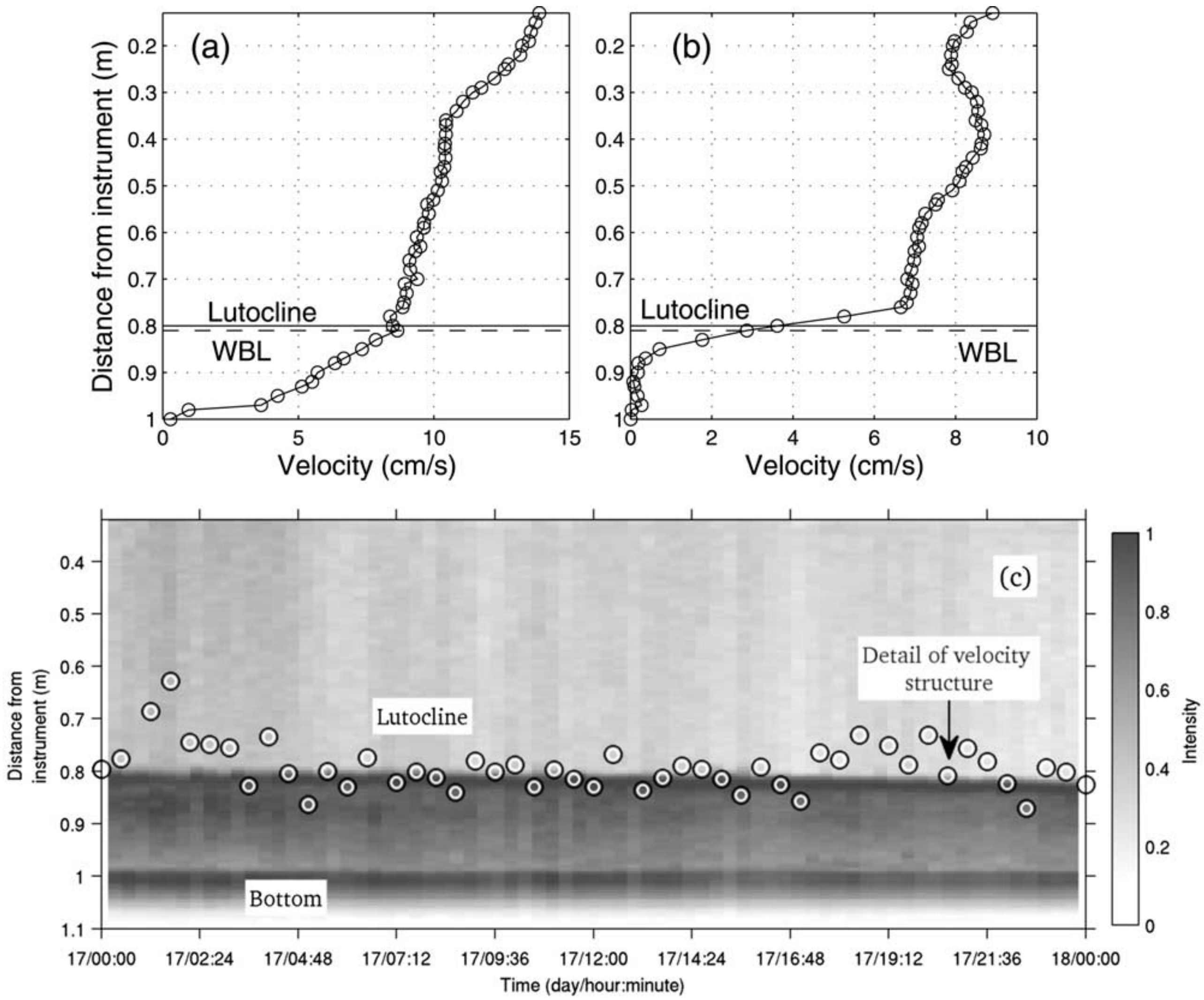

Figure 12. Detail vertical velocity structure and evolution of the lutocline at T2 during Experiment B, March 2006, for the period marked by the rectangle in Figure 11. Vertical profile of (a) RMS wave orbital velocity and (b) mean current velocity (10-min averages). (c) A detail of ABS backscatter intensity. Circles in Figure 12c represent the lutocline heights calculated using equation (3). Each dot represents a 10-min average. The arrow marks the measurement burst for which the vertical profiles in Figures 12a and 12b are shown.

from the ABS backscatter). The settling velocity was extrapolated from *Sheremet et al.* [2005, Figure 6a] for a hindered settling regime as $w_s = 2 \times 10^{-7}$ m/s.

[34] The results of the simulations are shown in Figure 12. As the parameters that characterize the mud suspension are kept constant throughout the simulation period, the trends in the simulation reflect only the variations of the characteristic amplitude and period of the wave forcing, which are estimated as 10-min averages, based on PC-ADP observations of wave velocity and wave power spectrum. The predictions of lutocline height based on equation (3) agree with the ABS observations, and also capture its slow settling trend in response to the decrease of the wave orbital velocity. The results support the hypothesis that the layer in Experiment B is also supported by wave-induced turbulence.

3.3. Seafloor Response

[35] Box cores taken during Experiment A, on 28 February and 14 March at both T1 and T2 can be used to constrain the stratal response to the fluid-mud layer events of 9–12 March. X-radiographs (Figure 13) show that by matching subbottom layers, surficial stratigraphy before the storm was incised to a depth of about 4 cm at T1 and 3 cm at T2, followed by deposition of a layer of coarser fabric signature (less opaque to X rays) that is about 2 cm thick at T1 and 3 cm at T2. Slight changes in stratigraphy at a site are likely expressions of small-scale spatial variability given that cores were taken over a 10-m radius of seafloor. The presence of macrofaunal burrows in both 14 March cores is testament to the rapid settlement of benthic biology poststorm. Radioisotope profiles from the same cores (Figure 14) also support the alteration of the upper seafloor

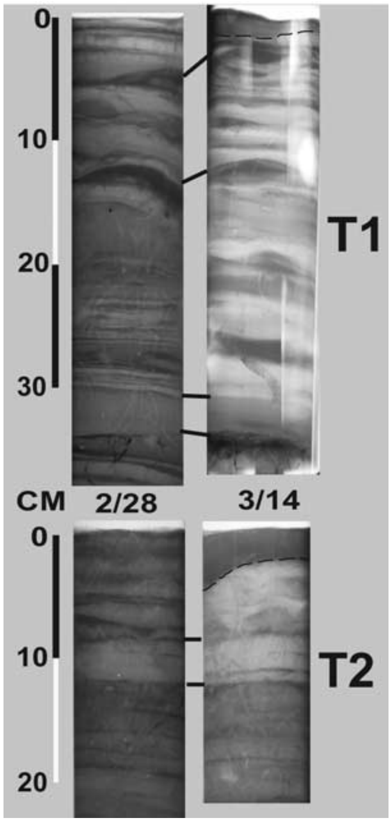

Figure 13. X-radiograph negatives (dark is coarser) of box cores taken at T1 and T2 sites prior to (28 February 2006) and following (14 March) the fluid-mud layer events associated with frontal passages during Experiment A. Matching subbottom stratal boundaries (guide lines between X-radiographs) suggests significant (3–4 cm) seafloor incision by the storm at both sites, and deposition of a relatively coarse event-layer deposit after the incision (base marked by dashed lines). White vertical areas in the T1 X-radiograph from 3/14 are artifacts of development.

by the frontal storm. The surficial layer on 14 March at both T1 and T2 has a lower excess ^{210}Pb activity. ^{7}Be changes are less definitive, but are slightly reduced in the upper cms at both sites. Activities of ^{137}Cs in this poststorm layer (not shown) are only 0.1–0.2 dpm/g: significantly lower than the prestorm surficial sediments (0.3–0.5 dpm/g). Given the different source functions for Pb (higher in particulates exposed to marine salinities) and Be and Cs (higher in particles from the river source [*Allison et al.*, 2000, 2005]) these reductions are likely a function of the coarser grain size in the poststorm event layer, given that particle-reactive radioisotopes are primarily adsorbed onto clay mineral surfaces. During Experiment B, box cores were collected on 15 March at T1 and T2, but no cores were collected upon recovery (31 March) that would allow for examination of surficial stratal changes. The 15 March cores (not shown) exhibit stratigraphies similar to the Experiment A sites, with centimeter-scale interbeds of silt and clay-rich intervals, but have an overall reduction in the opacity (coarseness) and thickness of the coarse interbeds. This reflects the relative finer character of the seafloor along the western delta front as has been observed previously. Radioisotope profiles of Pb, Cs, and Be (not shown) also support the fining: overall activities are higher than at the Experiment A sites.

[36] Although no bearing strength profiles were collected during experiments A and B, free-fall subsea penetrometer (STING) data were collected along two lines that cross the platform sites less than two months (3–5 May 2006) after Experiment B was concluded. These data (not shown) indicate that surficial strength is quite low (<40 kPa) in the vicinity of the platform sites to depths of 20–40 cm below bottom. In the areas where the pods were placed, bearing strengths at equivalent depths are generally lower along the Experiment B transect relative to the Experiment A transect, likely due to the finer sediments. Sediment bearing strength is typically 10 times the sediment shear strength determined from shear vane measurements [*Preston et al.*, 1999], so shear strength of these sediments is comparable to other low density fluid muds [*Narayana et al.*, 2008]. This correlation is consistent with recent evaluations of sediment strength in the Atchafalaya made with the penetrometer and with shear vane measurements A. H. Reed, unpublished data, 2008). This suggests that along Experiment B transect, predicted shear strengths ranged from 0.75 to 3.2 kPa, and along Experiment A transect, predicted shear strengths ranged from 1.0 to 8.6 kPa.

4. Summary

[37] Despite the absence of direct measurements of the bulk properties of the thin fluid-mud layers observed, the data collected by acoustic devices, supplemented with cores, penetrometer information, as well as suspension sensors in the overlying water column, and even platform position, allowed us to construct a consistent picture of sediment response to hydrodynamic forcing.

[38] On the topset/foreset of the Atchafalaya clinoform, two fluid-mud layers were recorded during Experiment A associated with a strong frontal passage, one dominated by bed liquefaction followed by sediment resuspension, and the other by advection and settling (in the waning phase of the storm), with a less evident liquefaction effect. The chain of events appears to be strongly correlated to swell energy levels (and less to short-wave activity):

[39] 1. At T1, preceding the first fluid-mud event, high wave orbital velocities penetrating at least 10 cm into the bed liquefy the bed (9 March 12:00, Figure 6); platform T1 began to settle.

[40] 2. As swell height grew over 1 m (first wave activity peak), a fluid-mud layer developed quickly (10 March, Event "1" in Figure 5), with flow velocities of about 5 cm/s, and directed seaward (downslope), together with the entire water column. Platform T1 settled by 10 cm.

[41] 3. In the wake of the front, a second fluid-mud layer developed (Event "2," 11 March, Figure 5) coinciding with a second, weaker peak of swell energy; flow velocities were slightly higher, directed still seaward and downslope, this time opposite to the water-column flow.

[42] While no information was available about sediment characteristics within the fluid-mud layers, a qualitative analysis based on models proposed by *Wright et al.* [2001], *Scully et al.* [2002], and others, yielded results that are consistent with wave-supported fluid-mud layers, flow-

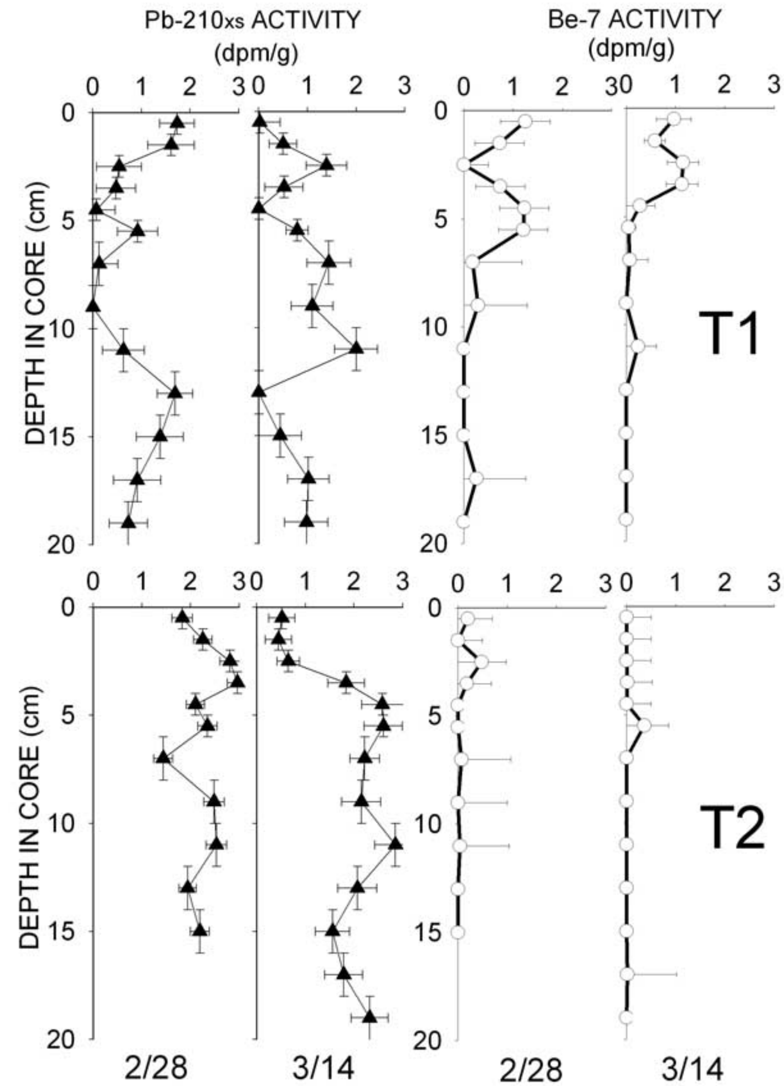

Figure 14. Downcore radiochemical profiles of excess ^{210}Pb and ^{7}Be of box cores taken at T1 and T2 sites prior to (28 February 2006) and following (14 March 2006) the fluid-mud layer events associated with frontal passages during Experiment A. These are the same cores depicted in X-radiographs in Figure 13. Note the reduced activity in the poststorm cores of Pb (and to a lesser extent Be), hypothesized to be due to incision of the higher-activity surface layers by the frontal storm and deposition of a coarser event layer during and following the passage of the fluid-mud sediment flows.

ing downslope on the clinoform. The event layer recorded in cores at T1/T2 taken 3 days after the second event is unsorted and shows no internal laminations that would be characteristic of turbidity flow deposits. Even sand-poor turbidites typically show deposition of normally graded silt-clay layers and are characteristic of higher slopes than that present (about 0.125%) between T1 and T2 [*Piper*, 1978; *Stow and Piper*, 1984; *Walsh and Nittrouer*, 2003].

[43] The observations collected during Experiment A suggest a specific, two-part sequence of wave-supported sediment transport events on a clinoform, triggered by pre-frontal energetic swells. The swells (e.g., peak on 9 March) liquefy the bed, likely over a large area (at least 4 km) on the outer topset and foreset of the clinoform, as indicated by the simultaneous motion and sinking of the T1 and T2 platforms. Prefrontal storm waves resuspend the sediment mobilized by liquefaction and a wave-supported, fluid-mud layer develops. As the front passes, the reversal of direction of wind and wind-forced currents from shoreward to seaward produces a temporary reduction in near-bed wave and current stresses, which results in turn in sediment settling and increased near-bed sediment content. This is readily resuspended during the second (weaker) storm pulse generating near-bed mud layers flowing downslope at about 5 cm/s, supported mainly by wave-induced turbulence.

[44] Only one (the most energetic) of the several storms observed during the two-month experiment resulted in this type of bed reworking, and it is not clear at this time what wave/current characteristics are responsible for this type of bed response. Swells seems to be the primary forcing, and one can assume, qualitatively, that the swell impact on the seafloor likely increases with decreasing frequency and

increasing energy. Another important factor must be the initial state of the bed (e.g., characterized by yield stress, shear strength, etc.). This points to the importance of the history of bed reworking (sediment thixotropy), and the influx of fresh riverine sediment.

[45] Liquefaction/resuspension is most intense at the outer site, consistent with a shoreward decrease in wave energy due to bottom-induced dissipation. Incipient, downslope-flowing fluid-mud layers likely form at (and perhaps even onshore of) the inner site (T2), and increase in thickness as they flow across the foreset surface. Greater accumulation is observed at T1 than T2 (Figure 14), suggesting the greatest accumulation would take place at the base of the clinoform due to a reduction in bed slope and increased water depths relative to wave base (8 m at clinoform base).

[46] Fluid muds observed during Experiment B on the western edge of the clinoform agree with previous observations of westward coastal currents ("Atchafalaya mud stream" [*Wells and Kemp*, 1981]). They last longer than 2 days, and show weaker flows (order of 1–3 cm/s), and appear to be controlled mainly by wave turbulence. The lack of information about the local bathymetry and the presence of the fluid mud at the time the tripods were deployed precludes us from drawing any conclusion about the origin and flow mechanism. It is possible that the Experiment B fluid mud was originated in the 7–14 March frontal storm that generated the Experiment A fluid mud. The fluid-mud layer could be slowly flowing down a local slope or/and pooling at the experiment site, being maintained by the wave-induced turbulence.

[47] Further field efforts are required, to understand the dynamics of wave-forced fluid-mud layers over a muddy, shallow clinoform, and their contribution to the overall sediment flux balance and clinoform progradation. Our observations of bed reworking during the 7–14 March storm contradict the assumption of a persistent, single-phase mud state, which forms the basis of most wave-mud interaction models. Although a detailed discussion of the significance of these observations with respect to wave propagation is deferred to a separate paper (A. S. Sheremet et al., manuscript in preparation, 2009), our observations suggest that future field investigations should make an effort to monitor bed-sediment state and near-bed suspended sediment concentration, in addition to detailed near-bed hydrodynamic measurements.

[48] **Acknowledgments.** This work was supported through Office of Naval Research funding of contracts N00014-07-1-0448 and N00014-07-1-0607 and Office of Naval Research base funding of the Naval Research Laboratory, program element 0601153N. Field data were collected with support by the Field Support Group of Coastal Studies Institute, Louisiana State University. The authors are grateful to the two anonymous reviewers for their insightful and constructive comments, and to Lacy Sherwood for providing the code for ambiguity resolution.

References

Allison, M. A., G. C. Kineke, E. S. Gordon, and M. A. Goñi (2000), Development and reworking of a seasonal flood deposit on the inner continental shelf off the Atchafalaya River, *Cont. Shelf Res.*, *20*, 2267–2294.

Allison, M. A., A. Sheremet, M. A. Goñi, and G. W. Stone (2005), Storm layer deposition on the Mississippi-Atchafalaya subaqueous delta generated by Hurricane Lili in 2002, *Cont. Shelf Res.*, *25*(18), 2213–2232.

Bea, R. G., S. G. Wright, P. Sircar, and A. Niedoroda (1983), Wave-induced slides in South Pass Block 70, Mississippi delta, *J. Geotech. Eng.*, *109*, 619–644.

Cacchoine, D. A., D. E. Drake, R. W. Kayen, R. W. Sternberg, G. C. Kineke, and G. B. Tate (1995), Measurements in the bottom boundary layer on the Amazon subaqueous delta, *Mar. Geol.*, *125*, 235–258.

Cutshall, N. H., I. L. Larsen, and C. R. Olsen (1983), Direct analysis of Pb-210 in sediment samples: Self-absorption corrections, *Nucl. Instrum. Methods*, *206*, 309–312.

DiMarco, S. F., and R. O. Reid (1998), Characterization of the principal tidal current constituents on the Texas-Louisiana shelf, *J. Geophys. Res.*, *103*, 3093–3109.

Draut, A. E., G. C. Kineke, O. K. Huh, J. M. I. Grymes, and K. A. Westphal (2005), Coastal mudflat accretion under energetic conditions, Louisiana chenier-plain coast, USA, *Mar. Geol.*, *214*, 27–47.

Hsu, T.-J., P. A. Traykovski, and G. C. Kineke (2007), On modeling boundary layer and gravity-driven fluid mud transport, *J. Geophys. Res.*, *112*, C04011, doi:10.1029/2006JC003719.

Kemp, G. P. (1986), Mud deposition at the shoreface: Wave and sediment dynamics on the chenier plain of Louisiana, Ph.D. thesis, 149 pp., Louisiana State Univ., Baton Rouge.

Kineke, G. C., and R. W. Sternberg (1992), Measurements of high concentration suspended sediments using the optical backscatterance sensor, *Mar. Geol.*, *108*, 253–258.

Kineke, G. C., E. E. Higgins, K. Hart, and D. Velasco (2006), Fine-sediment transport associated with cold front passages on the shallow shelf, Gulf of Mexico, *Cont. Shelf Res.*, *26*, 2073–2091.

Kranenburg, C. (1994), On the fractal structure of cohesive sediment aggregates, *Estuarine Coastal Shelf Sci.*, *39*, 451–460.

Lacy, J. R., and C. R. Sherwood (2004), Accuracy of a pulse-coherent acoustic Doppler profiler in a wave-dominated flow, *J. Atmos. Oceanic Technol.*, *21*, 1448–1461.

Michels, K. H., H. R. Kudrass, C. Hubshcer, A. Suckow, and M. Wiediecke (1998), The submarine delta of the Ganges-Brahmaputra: Cyclone-dominated sedimentation patterns, *Mar. Geol.*, *149*, 123–144.

Mossa, J. (1996), Sediment dynamics in the lowermost Mississippi river, *Eng. Geol.*, *45*, 457–479.

Narayana, A. C., C. F. Jago, P. Manojkumar, and R. Tatavarti (2008), Nearshore sediment characteristics and formation of mudbanks along the Kerala coast, southwest India, *Estuarine Coastal Shelf Sci.*, *78*, 341–352.

Neill, C. F., and M. A. Allison (2005), Subaqueous deltaic formation on the Atchafalaya Shelf, Louisiana, *Mar. Geol.*, *214*, 411–430.

Parsons, J. D., C. T. Friedrichs, P. A. Traykovski, D. Mohrig, J. Imran, J. P. M. Syvitski, G. Parker, P. Puig, J. L. Buttles, and M. H. García (2007), The mechanics of marine sediment gravity flows, in *Continental Margin Sedimentation: From Sediment Transport to Sequence Stratigraphy*, edited by C. A. Nittrouer et al., pp. 275–337, Blackwell, Malden, Mass.

Piper, D. J. W. (1978), Turbidite muds and silts on deep sea fans and abyssal plains, in *Sedimentation in Submarine Canyons, Fans, Trenches*, edited by D. J. Stanley and G. Kelling, pp. 163–175, Dowden Hutchinson Ross, Stroudsburg, Pa.

Preston, J. M., W. T. Collins, D. C. Mosher, R. H. Poeckert, and R. H. Kuwahara (1999), The strength of correlations between geotechnical variables and acoustic classifications, *Proc. MTS/IEEE Oceans*, *99*, 1123–1128.

Prior, D. B., and J. M. Coleman (1984), Submarine slope instability, in *Slope Instability*, edited by D. Brumsden and D. B. Prior, pp. 419–455, John Wiley, New York.

Roberts, H. H., R. D. Adams, and R. H. Cunningham (1980), Evolution of sand-dominant subaerial phase, Atchafalaya Delta, Louisiana, *Am. Assoc. Petrol. Geol. Bull.*, *64*, 264–279.

Roberts, H. H., O. K. Huh, S. A. Hsu, L. J. Rouse Jr., and D. A. Rickman (1989), Winter storm impacts on the chenier plain coast of southwestern Louisiana, *Trans. Gulf Coast Assoc. Geol. Soc.*, *39*, 515–522.

Scully, M. E., C. T. Friedrichs, and L. D. Wright (2002), Application of an analytical model of critically-stratified gravity-driven sediment transport and deposition on the Eel River continental shelf, Northern California, *Cont. Shelf Res.*, *22*, 1951–1974.

Sheremet, A., and G. W. Stone (2003), Observations of nearshore wave dissipation over muddy seabeds, *J. Geophys. Res.*, *108*(C11), 3357, doi:10.1029/2003JC001885.

Sheremet, A., A. J. Mehta, B. Liu, and G. W. Stone (2005), Wave-sediment interaction on a muddy inner shelf during Hurricane Claudette, *Estuarine Coastal Shelf Sci.*, *63*, 225–233.

Shlemon, R. J. (1975), Subaqueous delta formation—Atchafalaya Bay, Louisiana, in *Deltas*, edited by M. L. Broussard, pp. 209–221, Houston Geol. Soc., Houston, Tex.

Stow, D. A. V., and D. J. W. Piper (1984), Deep-water fine-grained sediments; history, methodology and terminology, *Geol. Soc. London Spec. Publ.*, *15*, 3–14.

Traykovski, P., W. R. Geyer, J. D. Irish, and J. F. Lynch (2000), The role of wave-induced density-driven fluid mud flows for cross-shelf transport on the Eel River continental shelf, *Cont. Shelf Res.*, *20*, 2113–2140.

Trowbridge, J. H., and G. C. Kineke (1994), Structure and dynamics of fluid muds on the Amazon continental shelf, *J. Geophys. Res.*, *99*, 865–874.

Van Heerden, I. L., and H. H. Roberts (1988), Facies development of the Atchafalaya Delta, Louisiana: A modern bayhead delta, *Am. Assoc. Petrol. Geol. Bull.*, *72*, 439–453.

Vinzon, S. B., and A. J. Mehta (1998), Mechanism for formation of lutocline by waves, *J. Waterw. Port Coastal Ocean Eng.*, *124*(3), 147–149.

Walker, N. A., and A. B. Hammack (2000), Impacts of winter storms on circulation and sediment transport: Atchafalaya-Vermilion Bay Region, Louisiana, U. S. A., *J. Coastal Res.*, *16*, 996–1010.

Walsh, J. P., and C. A. Nittrouer (2003), Contrasting styles of off-shelf sediment accumulation in New Guinea, *Mar. Geol.*, *196*, 105–125.

Walsh, J. P., C. A. Nittrouer, C. M. Palinkas, A. S. Ogston, R. W. Sternberg, and G. J. Brunskill (2004), Clinoform mechanics in the Gulf of Papua, New Guinea, *Cont. Shelf Res.*, *24*, 2487–2510.

Wells, J. T., and G. P. Kemp (1981), Atchafalaya mud stream and recent mudflat progradation: Louisiana chenier plain, *Trans. Gulf Coast Assoc. Geol. Soc.*, *31*, 409–416.

Wells, J. T., and H. H. Roberts (1980), Fluid mud dynamics and shoreline stabilization: Louisiana chenier plain, in *Proceedings of the Seventeenth International Coastal Engineering Conference*, vol. 17, pp. 1382–1401, Am. Soc. of Civ. Eng., Sydney, Australia.

Wright, L. D., C. T. Friedrichs, S. C. Kim, and M. E. Scully (2001), Effects of ambient currents and waves on gravity-driven sediment transport on continental shelves, *Mar. Geol.*, *175*, 25–45.

M. A. Allison, Institute for Geophysics, University of Texas at Austin, 10100 Burnet Road, R2200, Austin, TX 78758-4445, USA. (mallison@mail.utexas.edu)

K. T. Holland, Mapping, Charting, and Geodesy Branch, Naval Research Laboratory, Stennis Space Center, MS 39529, USA. (tholland@nrlssc.navy.mil)

S. Jaramillo and A. Sheremet, Civil and Coastal Engineering, University of Florida, 365 Weil Hall, P.O. Box 116580, Gainesville, FL 32611, USA. (sjaram1@ufl.edu; alex@coastal.ufl.edu)

A. H. Reed, Seafloor Sciences Branch, Naval Research Laboratory, Stennis Space Center, MS 39529, USA. (allen.reed@nrlssc.navy.mil)